Two Measure is Two Know: Calibration-free Full Duplex Monitoring for Software Radio Platforms

Jie Wang*, Jonathan Gornet*, Alex Orange[†], Leigh Stoller[†], Gary Wong[†],
Jacobus Van der Merwe[†], Sneha Kumar Kasera[†], and Neal Patwari*

*McKelvey School of Engineering, Washington University in St. Louis, St. Louis, Missouri, USA

[†]Kahlert School of Computing, University of Utah, Salt Lake City, Utah, USA

Abstract—Software-defined radio (SDR) platforms, despite being an enabler of spectrum and infrastructure sharing, must ensure that their transmitted signals comply with spectrum rules. Violations may occur because of malware, misconfiguration, bugs in software, or RF frontend nonlinearities. We present FDMonitor, a full-duplex monitoring system attached between a transmitter's power amplifier and its antenna to monitor and control each SDR in the Platform for Open Wireless Data-driven Experimental Research (POWDER), an open city-scale SDR-based testbed. FDMonitor uses a bidirectional coupler, a two-port receiver, and a new source separation algorithm to simultaneously and adaptively estimate the transmitted signal and the signal incident on the antenna. FDMonitor has been running on POWDER since 2021, monitoring 19 SDR platforms accessible by outside experimenters. Its closed-loop feature sends alerts in real time whenever a violation is observed, and automatically turns off the SDR as necessary. Our experimental results show that FDMonitor accurately separates signals across a range of critical parameters. We further validate the system-wide performance of FDMonitor with 27 months of observation. Over this period, it achieves a positive predictive value of 95%, with a total of 45 false alerts. Beyond its use on POWDER, FDMonitor, as a novel spectrum policy compliance solution, can be a key enabler of more dynamic sharing applications.

Index Terms—SDR wireless testbed, full-duplex monitoring, 27-month system evaluation.

I. INTRODUCTION

Today's open-access software-defined radio (SDR) wireless testbeds [1]–[5] are widely used across academia and industry for innovative spectrum research on topics such as dynamic spectrum access (DSA) [6] and radio dynamic zones (RDZ) [7]. As over-the-air experimentation of these technologies relies on spectrum coexistence with other spectrum applications, testbed operators must ensure that the transmitted signals comply with all spectrum policies and rules imposed by the operator or the national regulatory body, so that the testbed operator does not risk legal liability or being shut down. This paper presents the system that POWDER developed, tested, and is using to monitor the spectrum transmitted by each of its SDR platforms and to automatically turn off transmitters in violation.

While POWDER is open to users, users are not required to be open with their innovations, which adds complexity
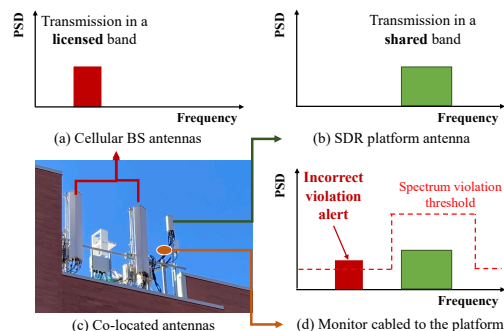
Fig. 1: A co-located base station's signal is incident to an SDR platform's antenna. If the monitor cannot separate the two signals, it may believe that its own SDR's transmitted signal is violating spectrum rules, which would be a false alarm.

to monitoring. POWDER users have bare-metal access to compute and SDR resources and can run arbitrary software stacks from physical to application layer. Full access gives users complete control. It further allows complete privacy of users' (potentially) proprietary waveforms and software stacks which can be commercial users' intellectual property. Our monitoring solution can not require access to user software.

Additionally, software-based monitoring is insufficient to ensure compliance. Power amplifiers (PAs) and radio frequency (RF) hardware in general have nonlinearities that can induce spurious emissions that violate spectrum rules [8]. The nonlinearities are difficult to characterize perfectly. As a result, the exact analog signal transmitted from the antenna is largely unknown. Further, monitoring only in software opens the door to attackers that could evade spectrum violation detection.

RF-based spectrum monitoring. For these reasons, this work proposes RF-based spectrum monitoring instead of software-based monitoring for full spectrum awareness. We describe our monitoring system as a **f**ull-**d**uplex **monitor** (FDMonitor) [9]. We use *full-duplex* to emphasize that it continuously and simultaneously estimates both the signal transmitted by the SDR and external signals incident to the SDR's antenna. As a result, FDMonitor simultaneously provides two critical functions to POWDER operators:

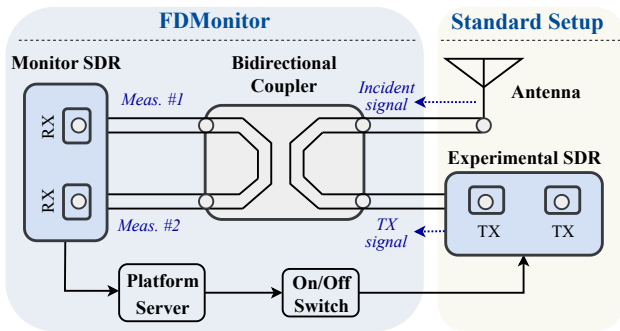- *User monitoring*: detect any violation of spectrum rules

Fig. 2: Architecture and the closed-loop control of FDMonitor, and the standard setup of its monitored SDR platform.

from transmitters in the testbed to ensure compliance.
- *Environment monitoring*: track potential interference from the environment to POWDER experimenters.

Being the source of interference could harm POWDER's relationships with other (licensed) wireless operators. In fact, POWDER has periodically received inquiries from licensed operators about interference they observe. Our monitoring datasets have been critical to demonstrate, as forensic evidence, that our platform was not the cause.

However, FDMonitor has to address a critical and significant challenge posed by co-located transmitted signals, as shown in Fig. 1. POWDER's base station antennas are deployed on cellular towers by a tower provider. The tower space is commonly leased to multiple operators, and antennas used by other mobile network operators (MNOs) may transmit at high power (e.g., 50 W) on the same tower. Since an antenna is a two-way device, some of a co-located MNO's signal impinges on the POWDER SDR's antenna. If we directly cable a spectrum monitor to the RF line before the antenna, it records both transmitted and incident signals, and cannot distinguish them. *In this case the monitor would wrongly conclude that the user is transmitting in the band owned by the MNO and, for spectrum compliance, turn off the POWDER SDR.*

Hardware design of FDMonitor. FDMonitor's bidirectional isolation hardware is the first step to address the co-located signal mixture problem. As shown in Fig. 2, a bidirectional coupler measures the forward and backward traveling signals on the RF path in two *different* linear combinations. However, a wideband bidirectional coupler does not perfectly isolate these two signals — the overall system can provide only 10–15 dB difference in the power of one source between the two coupled outputs. This is because RF subsystems are not perfectly matched over the wide bandwidths across which frequency-agile SDR platforms must be able to operate. Counterintuitively, the platform's transmitted signal and the incident signal are carried in *both* directions on the RF chain, so a *directional* coupler can only do so much.

Source Separation in FDMonitor. Separation of the transmitted and incident signals from the combinations above is the second step to realize accurate RF-based spectrum monitoring. The problems of such separation, however, are: (1) the exact linear mixture model is unknown and time-varying, and (2) neither transmitted nor incident signal is known to FDMonitor. Solutions like model calibration are time-intensive and require frequent manual effort.

We utilize *a frequency-domain independent component analysis (ICA)-based source separation algorithm* to address the problem. It requires no information about the model or the signals and estimates adaptively the transmitted signal, the incident signal, and the linear mixture model all on the fly. Our algorithm also tackles the resulting scaling and permutation ambiguities of ICA so that the separated signals are at correct power levels for violation detection and are identified correctly as "transmitted" or "incident".

Summary: The major contributions are as follows:
- Introduce the spectrum violation risks of SDR wireless testbeds and the need of shared SDR platform monitoring.
- Propose FDMonitor as a systems solution that separates mixed source signals, sends spectrum violation alerts, and automatically turns off the transmitters as necessary.
- Implement FDMonitor and deploy it on 19 shared SDR platforms available to researchers on POWDER.
- Evaluate FDMonitor's separation performance thoroughly over ranges of four RF parameters: modulation type, carrier frequency, bandwidth, and transmit power.
- FDMonitor has been running continuously on POWDER since 2021. It achieves a 95% positive predictive value of all reported violations over 27 months of operation.

II. RELATED WORK

Full-duplex monitoring of the shared SDR platforms is at the intersection of relevant research on (i) full-duplex communication and (ii) spectrum sensing.

A. Full-duplex Communication

Full-duplex communication [10]–[13] enables simultaneous transmission and reception in the same channel, and thus significantly increases spectral efficiency and network capacity [14]. Both full-duplex monitoring and full-duplex communication allow co-channel signal differentiation, but the former is focused on monitoring spectrum use, while the latter is for bidirectional communication. Self-Interference (SI) [15], i.e., the contamination of the received signal with the transmitted signal, is the biggest challenge for both. Proposed SI cancellation methods can be classified as: (i) propagation-domain, (ii) analog-domain, and (iii) digital-domain.

Propagation-domain SI cancellation methods isolate the transmit and receive chain carefully to electromagnetically suppress the SI before it shows up in the analog circuitry [10] via path loss enhancement [13], cross-polarization [16], transmit beamforming [17], or a circulator [18].

Analog-domain SI cancellation methods subtract a copy of the transmitted signal from received signals in the analog receive chain [10]. The methods can be classified as non-adaptive [19] or adaptive [20] depending on whether a time-varying environment is taken into consideration.

Digital-domain SI cancellation methods cancel SI from quantified received signals after the Analog-to-Digital Converter (ADC) [11]. A digital domain SI canceller first builds a baseband-equivalent model using the known transmit signal to capture everything between the DAC and ADC [13]. It then estimates linear and nonlinear components of SI based on the modeled channel to cancel the known transmitted signal.

Compared to these SI cancellation approaches, FDMonitor does not know the transmitted signal, and thus we cannot simply subtract it to estimate the other signal. FDMonitor first works in the propagation domain with its bidirectional coupler to enhance isolation between transmitted and incident signals. However, the isolation is insufficient due to matching across a very wide band of SDR operation. FDMonitor applies a blind frequency-domain source separation algorithm in the digital domain for further signal separation.

B. Spectrum sensing

A shared platform's transmission could be monitored by repurposed spectrum sensing. Spectrum sensing [21] was proposed to sense primary users for opportunistic spectrum reuse, but it is, in essence, an approach to remotely detect transmission. Repurposed spectrum sensing can be categorized as (i) direct sensing and (ii) cooperative sensing.

Direct sensing uses one node to locally sense a user's transmission [22]. It can be 1) transmitted signal prior-based sensing or 2) blind detection. The first type includes likelihood ratio test [21], cyclostationarity detection [23], waveform based sensing [24], and matched filtering [25]. These methods use priors such as signal distributions, cyclostationarity, and preamble and pilot patterns of the transmitted signals to be correlated with the received signal for signal presence detection. Blind detection, in contrast, does not require a prior [26]. It includes energy detection (ED) [27] or eigenvalue/covariance based detection [28]. ED measures the direct energy output whereas the latter uses the covariance matrix as an indicator of the received signal strength for presence classification.

Cooperative sensing utilizes measured signals sharing among collaborative radios to enhance the transmission sensing performance [21]. The spatial distribution of multiple nodes effectively avoids hidden node problems and ameliorates degradation due to multipath fading and shadowing [29]. While cooperative sensing can be centralized, distributed, and cluster-based [30], the fundamental sensing method is still direct sensing.

The above sensing techniques can be repurposed to monitor targeted transmissions of the shared SDR platform. However, it is unrealistic for us to require priors on the transmitted or incident signals, and blind detection will not be able to reliably separate co-channel signals. In comparison, FDMonitor can precisely separate and identify both the transmitted signal and incident signal, even if they are on the same channel. It does use two measurements, thus like cooperative methods, it benefits from redundant measurements.

Bidirectional sensing. The work described in [31] reports on spectrum monitoring using a bidirectional coupler. That
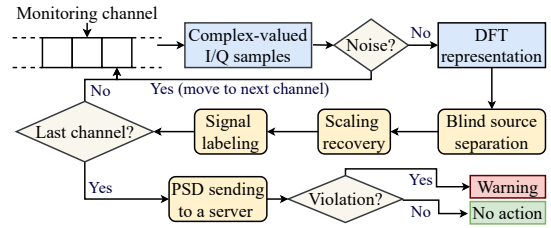

Fig. 3: System components and workflow of FDMonitor.

method assumes a known system model for estimating the transmitted signal. However, system model calibration requires time-intensive manual effort. Furthermore, weather changes result in system variations which, if not recalibrated, degrade the separation performance. Experimentally, we also find the approach cannot sufficiently separate the transmitted and incident signals when they overlap in the frequency domain. In comparison to [31], FDMonitor provides several new benefits: 1) it is robust across signal type, carrier frequency, bandwidth, and transmit power, 2) it enables mixing matrix estimation on the fly without system calibration, and 3) in addition to estimating the transmit signal, it *also* estimates the incident signal, which enables full-duplex monitoring.

III. SYSTEM DESIGN

We describe the design of FDMonitor, as shown in Fig. 3, that can separate signals without a signal prior. The inputs to FDMonitor are the In-phase and Quadrature (I/Q) sampled signals at the two receiver ports. Whenever the power in either receiver port is higher than the noise floor, we use the proposed algorithm to separate the signal into two sources. Given the Power Spectral Density (PSD) limits defined by the testbed operator, FDMonitor determines whether a violation occurred and reacts accordingly.

A. Problem Formulation

The overall goal of FDMonitor is to monitor the entire frequency range of the platform, in our case 100–6000 MHz. The monitor samples from one channel at a time, each with an RF bandwidth limited by the monitoring device capability, in our case 27.65 MHz. We describe, without loss of generality, how FDMonitor operates on *a single frequency channel*.

FDMonitor collects bidimensional samples $r_i(n)$ for sample $n = 0, 1, \ldots N - 1$ from ports $i = 0, 1$. Upon referring the source signals as $x_i(n)$ with $i = 0, 1$, we describe the bidimensional observations of the form:

$$\boldsymbol{r}(n) = \boldsymbol{A}\boldsymbol{x}(n) + \boldsymbol{v}(n), \tag{1}$$

where $\boldsymbol{r}(n) = [r_0(n), r_1(n)]^T$ and $\boldsymbol{v}(n)$ is zero-mean, uncorrelated additive Gaussian noise, i.e., $\boldsymbol{v}(n) \sim \mathcal{CN}(\boldsymbol{0}, \sigma^2 \boldsymbol{I})$. We now present the assumptions based on (1) and discuss the major problem that needs to be addressed.

Assumption 1. *The observations $\boldsymbol{r}(n)$ are a noisy instantaneous linear mixture of source signals from $\boldsymbol{x}(n)$, and the system matrix $\boldsymbol{A} \in \mathbb{C}^{2 \times 2}$ is assumed to be unknown.*

Signal mixtures can be instantaneous or convolutive [32], [33]. We assume the former due to the fact that FDMonitor collects I/Q samples within hundreds of microseconds, during which the linear model remains static. We assume no prior knowledge of the system matrix A because (1) calibration will not be required, and (2) weather and other changing conditions alter A in practice. Instead, FDMonitor can adaptively estimate the linear model on the fly.

Assumption 2. *Source signals $x_0(n)$ and $x_1(n)$, for $n = 0, 1, \ldots N - 1$, are mutually independent and unknown. At most one of the source signals is Gaussian distributed.*

As the transmitted and incident signals are from different sources: the SDR platform and outside world, one signal does not affect the other, leading to mutual independence. FDMonitor has no knowledge about the source signals as their properties are designed by platform users, and may even be proprietary and confidential. Given that digital signals are mostly non-Gaussian, assumption 2 holds.

Thus we design FDMonitor to solve the following problem:

Problem. *Given Assumptions 1, 2 and the linear model in (1), the challenge is to estimate transmitted and incident signals from the received bidimensional measurements only, which is commonly referred as Blind Source Separation (BSS) for an instantaneous linear mixture.*

B. Frequency-domain ICA Modeling

We introduce a well-known BSS technique, ICA, to address the problem. ICA approaches, according to [34], are identical to BSS solutions for instantaneous linear mixtures. They assume the same linear mixture framework as in (1) and require assumptions 1 and 2. ICA may be applied in either the time or frequency domain due to the linearity of Fourier transform. We adopt the frequency-domain ICA given the spectrum monitoring application of this work. In detail, complex-valued samples $r_i(n)$ for $i = 0, 1$ are first converted to frequency-domain components via Discrete Fourier Transform (DFT):

$$R_i(k) = \sum_{n=0}^{N-1} r_i(n) e^{-j\frac{2\pi}{N}kn}, \quad k = 0, 1, \ldots, N-1. \quad (2)$$

The linear model in (1) can then be rewritten in the frequency domain as:

$$R = AX + V, \quad (3)$$

where $R = [R_0, R_1]^T \in \mathbb{C}^{2 \times N}$ are the DFT components of raw samples and V in the frequency domain is still Gaussian distributed, $V \sim \mathcal{CN}(0, N\sigma^2 I)$ [35]. The objective of frequency-domain ICA is to estimate the system matrix A and source signals X in (3).

C. ICA for Source Separation

Joint Approximate Diagonalization of Eigen-matrices (JADE) [36] is selected among three well-known ICA methods as the source separation algorithm. The three ICA methods, as applicable to complex-valued signals, are considered in

this work: 1) Fast Independent Component Analysis (FastICA) [37]; 2) JADE [36]; and 3) Adaptable Complex Maximization of Nongaussianity (A-CMN) [38]. All three algorithms are widely used. However, FastICA and A-CMN require some prior knowledge of the source distribution in order to optimally choose the contrast function [38]. That prior distribution is not generally known by testbed operators, who want to accommodate as many wireless techniques as possible. As a result, the more adaptive JADE method is adopted in FDMonitor.

The separated estimates after JADE are $\tilde{X}$ and the mixing matrix estimate is $\tilde{A}$. Note that $\tilde{X}$ have neither the same magnitude as that of raw samples nor correct labeling of "transmitted" vs. "incident" due to two common ICA ambiguities we discuss in the next section.

D. Scaling and Permutation Alignment

ICA methods have two common problems: scaling ambiguities and permutation ambiguities. First, ICA solutions are scaled by an unknown constant. Second, the two signal estimates are arbitrarily assigned, thus it is not known which signal was "transmitted" and which was "incident". These ambiguities impose great challenges on violation detection as FDMonitor does not know which estimate to look at for violation detection and which for environmental spectrum monitoring.

Assume that the two ICA estimates are each scaled by a multiplicative factor and may be permuted (i.e., swapped). These changes are modeled via the mixing matrix as:

$$\tilde{A} \longleftarrow \Lambda \hat{A} W, \quad (4)$$

where Λ is a diagonal scaling matrix. $\hat{A}$ is the ultimate mixing matrix to be obtained, and W is *either* the 2×2 identity matrix, or if it is permuted, the 2×2 exchange matrix $J_2 \triangleq \begin{bmatrix} 0 & 1 \\ 1 & 0 \end{bmatrix}$.

In the next sections, we first recover the scale via the estimated mixing matrix and address permutation ambiguity using correlation coefficients and power differences.

1) Scaling Alignment: We observe, from (4), that $\tilde{A}$ having a norm larger than 1 essentially causes the scaling ambiguity challenge. To recover the scale, we first diagonalize the mixing matrix $\tilde{A}$ to obtain a complex-valued diagonal matrix $\Delta(\tilde{A})$:

$$\Delta(\tilde{A}) = \text{Diag}\{\tilde{A}\}. \quad (5)$$

The correct power level of the two estimates is then:

$$\hat{X}(k) = \Delta(\tilde{A})\tilde{X}(k), \, k = 0, 1, \ldots, N - 1. \quad (6)$$

2) Permutation Alignment: To simplify the problem, we first hypothesize the following: "transmitted" $\leftrightarrow \hat{X}_0(k)$, "incident" $\leftrightarrow \hat{X}_1(k)$. The permutation is incorrect if the hypothesis is false. As we know that $R_0(k)$ from port 0 detects more of the transmitted signal than port 1 does given by FDMonitor's directionality, we first use the Pearson correlation coefficient [39] to test the hypothesis:

$$\text{corr}(|\hat{X}_i|, |\tilde{R}_j|) = \frac{\text{Cov}\{|\hat{X}_i|, |\tilde{R}_j|\}}{\sigma_{|\hat{X}_i|}\sigma_{|\tilde{R}_j|}}, \quad i, j = 0, 1, \quad (7)$$
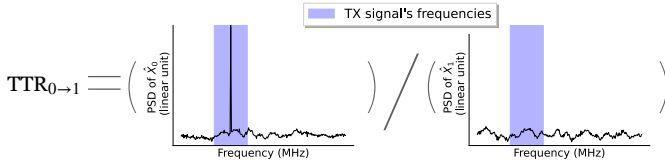
Fig. 4: The evaluation metric $\text{TTR}_{0\rightarrow 1}$ is defined as the ratio between the PSD of $\hat{X}_0$ and $\hat{X}_1$ averaged across the TX signal's frequencies (▅). Higher TTR shows better separation due to more transmit power in $\hat{X}_0$ and much less in $\hat{X}_1$.

where $|\cdot|$ denotes the magnitude of the complex value. $\text{Cov}\{\cdot\}$ is the covariance and σ is the standard deviation operator, calculated over all frequency samples k. We then are able to align the results based on the maximum of the four correlation values:

$$\hat{i}, \hat{j} = \arg\max_{i,j\in\{0,1\}} \text{corr}(|\hat{X}_i|, |\tilde{R}_j|). \tag{8}$$

If indices $\hat{i} = \hat{j}$, regardless of the value, we accept the hypothesis. Otherwise, we multiply $\hat{X}$ by the exchange matrix J_2 to swap them back.

The above solution applies to all but *source signals of similar power spectra shapes* as the correlation coefficients, in this case, are closely high and hence unreliable. As a result, we propose to further align permutation via power maximum between $\tilde{R}$ and $\hat{X}$ if the correlation coefficients fall out of the 95% confidence interval. Specifically, If $\tilde{R}_0$ has more power than $\tilde{R}_1$, $\hat{X}_0$ should correspondingly have higher magnitude than $\hat{X}_1$. Therefore $\tilde{R}_j$ and $\hat{X}_i$ with higher power are matched.

3) Mixing Matrix Adjustment: Adjustments of the estimated mixing matrix $\tilde{A}$ are needed to properly account for the changes we made for scaling and permutation alignment above. The final estimated mixing matrix is:

$$\hat{A} = (\Delta(\tilde{A}))^{-1}\tilde{A}W \tag{9}$$

where $(\Delta(\tilde{A}))^{-1}$ is the scaling recovery matrix and W is the permutation recovery matrix: if permutation occurs, $W = J_2$, otherwise it is the 2×2 identity matrix.

E. Performance evaluation

We propose a new evaluation metric, as shown in Fig. 4, to quantitatively evaluate FDMonitor's separation performance. The principle is that we do not want the algorithm to "blame" the user for the incident signal, nor do we want to corrupt the incident signal estimate with the user's transmitted signal.
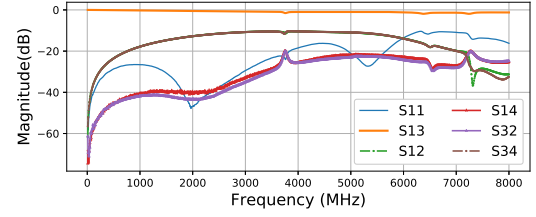
To define the metric, we define a frequency channel (set) $\mathcal{B}_{Tx}$ to contain frequency indices in which the node is transmitting and set $\mathcal{B}_{In}$ to contain frequency indices in which there is the incident signal. We compute the average PSDs of these signals in estimated signals $\hat{X}_i(k)$, for $i = 0, 1$, as:

$$P_i[Tx] = \frac{1}{|\mathcal{B}_{Tx}|}\sum_{k\in\mathcal{B}_{Tx}} |\hat{X}_i(k)|^2$$

$$P_i[In] = \frac{1}{|\mathcal{B}_{In}|}\sum_{k\in\mathcal{B}_{In}} |\hat{X}_i(k)|^2. \tag{10}$$
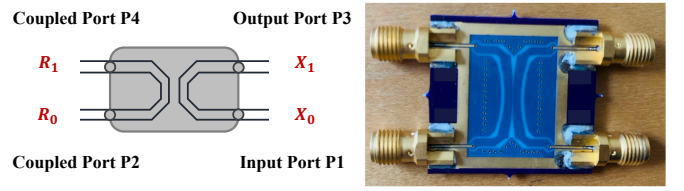
(a) Port diagram   (b) PCB realization

(c) Measured S-parameters

Fig. 5: The custom Bidirectional coupler. While extremely wideband and low loss, the isolation between coupled ports can be as low as 10 dB.

We then define the *Transmit in port 0 to Transmit in port 1 Ratio (TTR)* and the *Incident in port 1 to Incident in port 0 Ratio (IIR)* as:

$$\text{TTR}_{0\rightarrow 1} = \frac{P_0[Tx]}{P_1[Tx]}, \quad \text{IIR}_{1\rightarrow 0} = \frac{P_1[In]}{P_0[In]}. \tag{11}$$

Similar to the signal-to-interference ratio (SIR), our TTR and IIR values measure a power ratio. However, TTR and IIR do not require exact knowledge of the true transmitted and incident signals $X_0(k)$ and $X_1(k)$ for all k, which is unavailable, even during experiments. Our metrics, TTR and IIR, focus specifically on the isolation performance of FDMonitor rather than the quality of $\hat{X}_0(k)$ and $\hat{X}_1(k)$ individually.

IV. IMPLEMENTATION

In this section, we present the implementation of FDMonitor on our large-scale wireless testbed, POWDER.

A. Monitoring Hardware

We use the following hardware in our experiments: (1) an SDR transmitter and incidental source each controlled via USB by an Intel NUC computer, (2) our custom bidirectional coupler connected between the TX port and antenna, (3) the monitor node connected to the two output ports of the bidirectional coupler, and (4) a wide-band antenna

We use a NUC, a small-form-factor PC with an Intel Core I7-8650 processor and 32 GB of DDR4 RAM, running Ubuntu 18.04 LTS. Our monitor and experimental SDR are both NI USRP B210s which are able to transmit and receive in the spectrum range from 70–6000 MHz [40], with a sample rate up to 61 MSps. The antenna used is a TAOGLAS wide-band 4G LTE I-Bar, effective across a 698-6000 MHz band [41].

A critical component of FDMonitor, a bidirectional coupler, is designed and built as shown in Fig. 5a and 5b. It has

four ports: P1 and P3 are input and output ports representing direct transmission whereas P2 and P4 are coupled ports which can capture mixed signals at different scales. To show the directionality of the coupler when it is isolated, we measure its S-parameters across the 100–6000 MHz frequency range, as shown in Fig. 5c. S_{11} shows low return loss, below -10 dB across the band. S_{13} is close to 0 for the wide spectrum, indicating little power loss of the direct transmit signal from P1 to P3. In addition, S_{12} and S_{14} show that P2 and P4 receive a copy of the transmitted signal that is at least 10 dB and 20 dB down from the transmitted power, respectively. Likewise, S_{32} and S_{34} show that the samples collected in P4 and P2 are at least 20 dB and 10 dB down from the incident signal power.

B. Monitoring Software

To monitor the entire 100–6000 MHz range, FDMonitor divides the spectrum into multiple smaller frequency channels. Issues with NI USRP B210s sometimes result in invalid samples when operating at its maximum sampling rate, thus we use a rate of 27.65 MSps, a factor of 0.9 of its maximum dual-mode sampling rate. To cover the entire monitoring spectrum, 214 monitoring channels must be iterated through. For the results here, in each channel, $N = 2 \times 10^4$ complex-valued samples are collected by FDMonitor for source separation and mixing matrix estimation.

The FDMonitor procedure is detailed in Algorithm 1. Note that PSD limits may be user-dependent, and we assume that they are known to the algorithm. Our implementation notifies the user and staff of the problem and automatically shuts off the transmitter if the violation persists.

V. Results

In this section, experimental results of FDMonitor are presented using the setup shown in Fig. 2.

Baseline method. We use *System Matrix Calibration (SMC)* [31] as a baseline to compare to FDMonitor. SMC works as follows. SMC first calibrates the system matrix, at each frequency bin, by placing the system in an RF isolation chamber. In detail, a known signal is first transmitted by the experimental SDR and is received by the monitoring system at two ports. A spectrum analyzer captures the actual transmitted signal X_0. As the incident signal is zero, half of the mixing matrix can be estimated by comparing the measurements R and X_0. Similarly, by setting $X_0 = 0$ and transmitting a signal from an incident source (as measured by a spectrum analyzer), the other half of the mixing matrix is obtained. The calibrated linear model is then inverted and is used, during operation, for signal separation and identification.

A. Source Separation of FDMonitor

Our first series of experiments are designed to answer a critical question: **Can FDMonitor separate and identify transmitted vs. incident signals of different modulations, center frequencies and bandwidths, and relative power levels?** We conduct multiple controlled experiments, where we set the transmitted signal and create an environmental signal that impinges on the platform antenna, to answer this question.

Algorithm 1: Algorithmic Operation of FDMonitor

Result: TX/incident signals, alert notification
Initialize user PSD limits vs. frequency;
Initialize the list of channel center frequencies f_{list};
while *True* **do**
 for f *in* f_{list} **do**
  Sample $r_i(n)$ for $i = 0, 1$ & $n = 0 \dots N - 1$;
  $R_i(k) \leftarrow \text{FFT}\{r_i(n), i = 0, 1\}$; /* III-B */
  $\tilde{X}(k), \tilde{A} \leftarrow \text{JADE}\{R(k)\}$; /* III-C */
  $\hat{X} \leftarrow \Delta(\tilde{A})\tilde{X}(k)$;
  $\hat{A} \leftarrow \left(\Delta(\tilde{A})\right)^{-1} \tilde{A}$; /* Scaling */
  if $corr(|\hat{X}_i|, |\tilde{R_m}|) > 0.95 \,\forall i, m = 0, 1$ **then**
   $i \leftarrow \arg\max_i(|\hat{X}_i|, \quad i = 0, 1$
   ; $m \leftarrow \arg\max_m(|\tilde{R_m}|), \quad m = 0, 1$;
  else
   $i, m \leftarrow \arg\max_{i,m} \text{cor}(|\hat{X}_i|, |\tilde{R_m}|)$;
  end
  if $i \neq m$ **then**
   $\hat{X}(k) = J_2 \cdot \hat{X}(k)$;
   $\hat{A} = J_2 \cdot \hat{A}$; /* Permutation */
  end
 end
 Concatenate $\hat{X}(k)$ for all frequency channels f;
 Compute $\text{PSD} = 10 \log_{10} |\hat{X}_0(k)|^2$;
 if *PSD > user PSD limits* **then**
  Notify & send PSD graph to user & staff;
 end
end

Modulation Types		Reference		SMC		FDMonitor	
Transmitted signals	Incident signals	TTR (dB)	IIR (dB)	TTR (dB)	IIR (dB)	TTR (dB)	IIR (dB)
CW	OFDM	13.30	7.21	30.92	3.54	**30.95**	**19.60**
OFDM	CW	12.56	6.91	22.61	7.39	**29.60**	**18.14**
CW	BPSK	13.38	6.02	30.24	4.48	**30.26**	**16.33**
BPSK	CW	12.55	6.40	20.06	8.32	**28.06**	**18.65**
OFDM	BPSK	13.12	6.33	22.64	5.60	**29.68**	**16.36**
BPSK	OFDM	13.17	7.76	20.48	3.85	**28.48**	**19.48**

TABLE I: TTR and IIR for signals of three modulation types. SMC increases signal isolation in CW scenarios only. FDMonitor provides more isolation across all signal types.

1) Signal Type: An experiment is conducted in which an OFDM signal is transmitted at 3670 MHz and a BPSK signal is incident at 3659 MHz. Both have a bandwidth of 4 MHz. The results in Fig. 6a plot the PSD of R_0 and R_1 on the left, showing them at different power levels due to the directionality of the coupler. The right plots of Fig. 6a show that FDMonitor enables accurate separation of transmitted and incident signals, and also correct labeling of the two.

We further compare FDMonitor to SMC with typical digital signal types, CW, BPSK, and OFDM, using TTR and IIR.
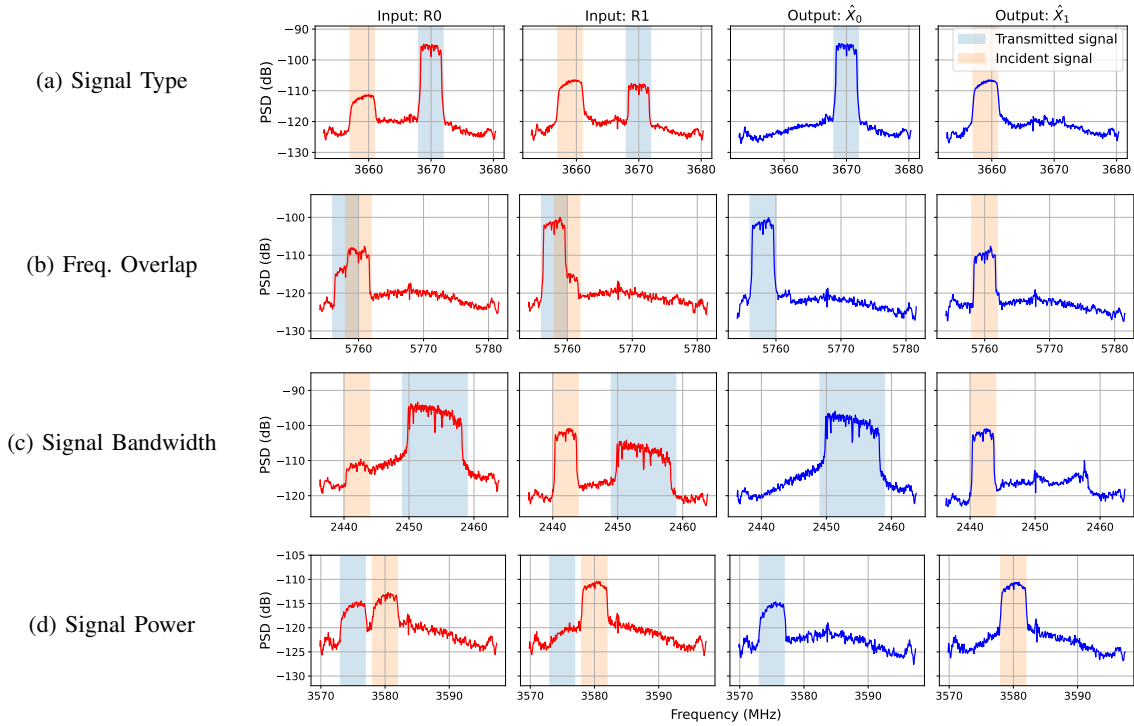
Fig. 6: FDMonitor's separation and identification under four RF settings: (a) OFDM transmitted signal and BPSK incident signal, (b) Overlapping OFDM signals, (c) signals of 10 MHz and 4 MHz bandwidths, and (d) BPSK signals at similar power levels, -115 and -113 dB. Each row shows the PSDs of raw samples, R_0 and R_1, and the PSDs of separation estimates, $\hat{X}_0$ and $\hat{X}_1$, all in dB scale. The results present that FDMonitor can accurately and robustly separate and identify transmitted vs. incident signals of different modulations, carrier frequencies, bandwidths, and relative power levels.
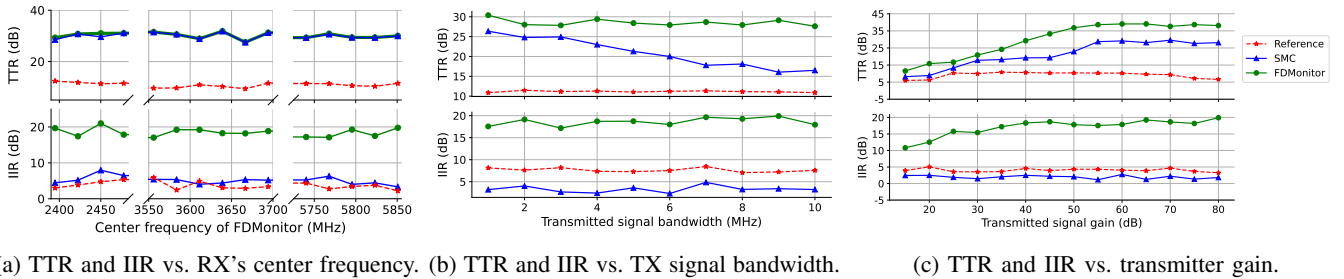

(a) TTR and IIR vs. RX's center frequency. (b) TTR and IIR vs. TX signal bandwidth. (c) TTR and IIR vs. transmitter gain.

Fig. 7: TTR(transmit signal separation) and IIR(incident signal separation) comparisons between FDMonitor and SMC. (a) *Receiver's center frequency*: both methods present similar TTR increase, but FDMonitor results in superior IIR. (b) *Transmitted signal bandwidth*: FDMonitor is consistent across bandwidths whereas SMC degrades as bandwidth increases. (c) *Transmitter gain*: FDMonitor improves both while SMC reduces IIR with the increasing gain.

The results in Table I show that both methods increase the isolation of the transmitted signal in $\hat{X}_1$. However, we observe two disadvantages of SMC. First, it can only improve TTR as much as FDMonitor in CW transmission scenarios. Large TTR differences in modulated transmitted signals expose the inability of SMC to remove the transmitted signal from $\hat{X}_1$. Secondly, SMC shows only a small IIR increase when the incident signal is CW, but inadvertently reduces the isolation for other signals.

2) Carrier and Center Frequency: Can FDMonitor separate signals that overlap in the frequency domain? We experi-

ment with two overlapping OFDM signals: an incident signal (5758–5762 MHz) and a transmitted signal (5756–5760 MHz) that overlap between 5758–5760 MHz. The separation results in Fig. 6b show the complete removal of the incident signal from $\hat{X}_0$, and the complete removal of the transmitted signal from $\hat{X}_1$. Furthermore, our experience indicates that FDMonitor can separate signals that fully overlap in the frequency domain as long as the modulations are sufficiently different.

To check the separation performance across center frequency at the FDMonitor, experiments are conducted in the

2.4 GHz and 5.8 GHz ISM and 3.6 GHz CBRS bands, while transmitting non-overlapping CW signals. Fig. 7a shows that both methods increase the TTR across frequency, which means little impact of center frequency on either algorithm. However, the large difference shown in IIR indicates poor incident signal separation of SMC and robust estimation via FDMonitor.

3) Signal Bandwidth: The transmitted and incident signal properties are unknown to FDMonitor, and might both occupy large bandwidths. We next run tests to explore how the performance of FDMonitor is affected by signal bandwidth.

The experiment considers two OFDM signals: the transmitted signal is 10 MHz wide, centered at 2454 MHz, while the incident signal is at 2442 MHz with 4 MHz bandwidth. Fig. 6c shows the incident signal is removed from $\hat{X}_0$. Equivalently, the transmitted signal has been mostly eliminated in $\hat{X}_1$. Notably, 4 dB of the edges of the transmitted signal remains in $\hat{X}_1$. Additionally, the spike at 2458 MHz was verified to be an environmental interference signal. This observation indicates that FDMonitor can perform source separation in the presence of multiple incident signals.

Fig. 7b shows how TTR and IIR change as the transmitted signal bandwidth varies from 1 to 10 MHz (10 MHz is the maximum bandwidth a user can reserve for one experiment on the POWDER testbed). FDMonitor is stable across bandwidths, but SMC demonstrates decreasing TTR with higher bandwidth. Additionally, the IIR for SMC is stable but much lower than the IIR reference, whereas FDMonitor produces higher IIRs. Reduced IIR means there is a higher level of the incident signal in $\hat{X}_0$ than in R_0, a negative result.

4) Signal Power: Power difference is used for solving the permutation ambiguity (Section III-D). However, close power levels, in theory, could confuse FDMonitor. Thus, we present FDMonitor's performance as a function of signal power.

Fig. 6d shows the separation of two BPSK signals at close power levels, with the transmitted signal centered at 3575 MHz and the incident signal centered at 3580 MHz. As the transmitted signal gain is low, it is nearly invisible in the PSD of $R_1(k)$. Despite the low power transmitted signal, the results show that FDMonitor accurately estimates and identifies each signal.

Finally, we change the transmitter gain for separation performance evaluation, as shown in Fig. 7c. The TTR and IIR reference are approximately 6 and 4 dB. After running SMC and FDMonitor, we make the following observations: (1) TTR for both methods increases while gain increases from 10 to 55 dB; (2) FDMonitor obtains higher TTR than SMC at each gain setting; (3) SMC provides IIR around 2–3 dB lower than the reference while FDMonitor increases IIR by 7-16 dB.

B. Algorithm Efficiency

We compare the two systems' efficiency via latency. Latency in our work refers to the elapsed time for frequency tuning, data collection, and further analysis. Wideband monitoring of RF transmissions involves two main components, frequency sweeping and source separation. The former tunes the center frequency of the receiver while the latter provides transmitted
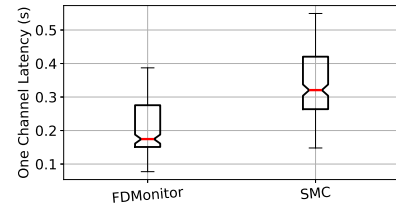

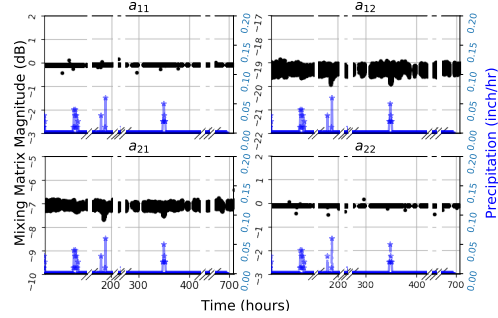Fig. 8: Latency of FDMonitor and SMC of one channel.

Fig. 9: Mixing matrix magnitude over 105 hrs, with precipitation data. The magnitudes of matrix values are stable, but a_{12} & a_{21} change while surfaces are wet due to rain.

signal estimation in each 27.65 MHz channel. To assess the methods in terms of efficiency, latency is measured in each monitoring channel. Fig. 8 shows that, for monitoring one channel, the median latency of FDMonitor is 0.17 s whereas SMC requires 0.32 s. Given the median latency, the total time spent by FDMonitor to sweep the 100-6000 MHz spectrum is 36.4 s, half the latency of SMC.

C. Mixing Matrix Evaluation

We further evaluate the system performance via the mixing matrix $\hat{A} \in \mathbb{C}^{2 \times 2}$, which describes the linear system model for source separation, which is estimated on the fly. We collect mixing matrix and precipitation data for 29 days while continuously transmitting CW signals from both sources.

Fig. 9 shows the mixing matrix magnitude vs. precipitation and monitoring hours. First, we observe that the matrix magnitude is relatively stable across 29 days. Both a_{11} and a_{22} are centered at 0.01 dB with 0.002 dB standard deviation. Noisier a_{12} and a_{21} are around -19.29 and -7.10 dB respectively with 0.094 and 0.075 dB standard deviation. Additionally, we notice that the matrix varies with rainfall. At around 72, 187 and 348 hours, the magnitude of a_{12} and a_{21} decreases when rain starts and later goes back to the same pre-rain level. This can be explained by the change in the radio propagation environment for wet vs. dry surfaces [42]. This is another reason why the baseline SMC method, which learns the system matrix only once during calibration, is not robust compared to FDMonitor.

D. Adversarial Behavior

If FDMonitor sequentially monitors frequency channels to cover the entire 100-6000 MHz band, adversarial users

Type	False positives: 45 emails		True positives: 944 emails				
Rate	False discovery rate (FDR): 4.6%		Positive predictive value (PPV): 95.4%				
Cause	Bug: Spectrum declaration lost	Permutation ambiguity	No spectrum declaration/ TX-declaration mismatch	High gain induced harmonics	Signal spillover	Intermodulation distortions	System testing
Rate	62.2%	37.8%	58.2%	23.0%	0.8%	13.1%	4.9%

TABLE II: FDMonitor alert accuracy during continuous monitoring of 19 shared SDR platforms for 27 months since 2021.
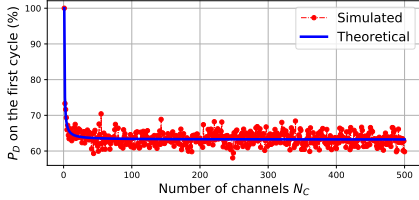

Fig. 10: Probability of detecting violation in the first cycle.

can potentially transmit in violation while hopping between channels to avoid detection. To model adversarial behaviors, we use the following notation: 1) ΔT is the time duration to monitor one channel, 2) N_C is the total number of channels (in our case, 214), and 3) T denotes the cycle number, where each cycle corresponds to monitoring all N_C channels.

Attack model We propose the following attack model: 1) an attacker can use any channel at any given time, 2) in each time slot ΔT, an attacker chooses 1 of the N_C channels to transmit, 3) an attacker does not know which channel is being monitored.

Countermeasure To address this attack model, FDMonitor can no longer use a predictable monitoring scheme. Instead, we propose a countermeasure that randomizes the order: 1) in each monitoring cycle, FDMonitor generates a random permuted channel sequence of length N_C for spectrum monitoring, 3) all channels are measured by FDMonitor in each cycle. *The probability of first detecting an attacker at cycle T using the proposed countermeasure is*:

$$ P_D(T) = \left(\frac{N_C - 1}{N_C} \right)^{N_C(T-1)} \left[1 - \left(\frac{N_C - 1}{N_C} \right)^{N_C} \right]. \quad (12) $$

$P_D(1)$ asymptotically converges to $1 - \frac{1}{e}$ or 63% as $N_C \to \infty$. The average number of cycles for attacker detection is $1/P_D(1)$, which for high N_C is 1.58 cycles. The proof is omitted due to space constraints. For validation, we show in Fig. 10 results of a simulation run 10^4 times at each N_C. In FDMonitor, $N_C = 214$, and thus $P_D(1) = 65.18\%$.

We describe one attack model above and will investigate more adversarial behaviors in our future work.

E. System-wide 27-Month Deployment

FDMonitor has been continuously monitoring 19 SDR platforms on the testbed, all deployed at different geographical locations, for 27 months since 2021. We evaluate its system-wide performance by investigating each violation alarm it generates during the period, and considering the alarm accuracy. A violation alarm notifies the user via email of detected signals being transmitted outside the declared spectrum. It can be a true detection of RF emission misbehavior, or a false alarm if the alert did not correspond to a user violating spectrum rules. We store measurements from each alert and request information from the user about their setup in order to determine the ground truth about spectrum use.

Table II shows our analysis of the 989 total alerts. In summary, we observe only 45 false alarms, among which 28 alerts occurred because the user-declared frequency was, due to a software error, not recorded to the FDMonitor user PSD limits database. The other 17 false discovery emails were triggered by incorrectly resolved permutation ambiguities. Even so, the 95.4% positive predictive value (PPV) represents high accuracy and robustness of FDMonitor across a large variety of real users, their signals, and the varying weather seen by the platform.

No false negative cases (when a user's violating transmission is not detected as a violation) have been reported by POWDER users, and there were no false negatives in our experimental violation tests. Future work should investigate other methods to quantify the false negative rate during normal user operation.

Finally, we note that FDMonitor ran about 1.9 million times in the 27 months. 45 false discoveries in this period correspond to a false alarm *rate* of approximately 2×10^{-5}.

VI. Discussion

We describe some limitations of FDMonitor and discuss the implications for future research.

Non-Gaussian constraint. One constraint of FDMonitor is Assumption 2 that at most one of the sources is Gaussian. One possible solution is that, if both signals are found to be Gaussian, FDMonitor could use a recently estimated system matrix $\hat{A}$ for separation instead of estimating it on the fly.

Generalization to MIMO platforms. Currently one FDMonitor is needed for each transmit antenna as it relies on a bidirectional coupler to separate the transmit and incident signal to that antenna. This could be a scaling problem for MIMO platforms. However, future work could use a $(N+1)$-directional coupler for monitoring N-antenna MIMO platforms assuming that the incident signal appears in different linear combinations on all antennas. By doing so, $N+1$ rather than $2N$ inputs would be needed for MIMO separation.

VII. Conclusion

This paper proposes, implements, and reports on FDMonitor, a robust and continuous full-duplex monitoring system for effective supervision of 19 SDR platforms' transmissions and environmental use of spectrum. FDMonitor uses a new frequency-domain source separation algorithm to distinguish signals of the SDR platform from those incident on the antenna. Critically, our approach does not require extensive calibration, which would be very challenging to implement at the rate at which calibration becomes obsolete. Its performance is extensively validated with four different types of RF signal experiments, across communication signal modulations, carrier frequency, bandwidth, and transmit power. We further validate 27 months of live system performance, which generates a low 4.6% FDR, with 45 false alerts.

References

[1] "Platforms for advanced wireless research (PAWR) program," 2018. https://advancedwireless.org/.

[2] "5G PPP platforms cartography," 2018. https://5g-ppp.eu/5g-ppp-platforms-cartography/.

[3] "Bristol Is Open," 2013. https://www.bristol.gov.uk/policies-plans-strategies/bristol-is-open.

[4] "The ADRENALINE testbed," 2017. http://networks.cttc.es/ons/adrenaline/.

[5] "Open-access research testbed for next-generation wireless networks (ORBIT)," 2005. https://www.orbit-lab.org/.

[6] S. Bhattarai, J.-M. J. Park, B. Gao, K. Bian, and W. Lehr, "An overview of dynamic spectrum sharing: Ongoing initiatives, challenges, and a roadmap for future research," *IEEE Transactions on Cognitive Communications and Networking*, vol. 2, no. 2, pp. 110–128, 2016.

[7] M. Zheleva, C. R. Anderson, M. Aksoy, J. T. Johnson, H. Affinnih, and C. G. DePree, "Radio dynamic zones: Motivations, challenges, and opportunities to catalyze spectrum coexistence," *IEEE Communications Magazine*, vol. 61, no. 6, pp. 156–162, 2023.

[8] J. Vuolevi and T. Rahkonen, *Distortion in RF power amplifiers*. Artech House, 2003.

[9] J. Wang, B. C. Terry, and L. Stoller, "GitLab repository of the proposed full-duplex monitoring system." https://gitlab.flux.utah.edu/Jie_Wang/spectrum-monitor/-/tree/code_merge, 2022.

[10] A. Sabharwal, P. Schniter, D. Guo, D. W. Bliss, S. Rangarajan, and R. Wichman, "In-band full-duplex wireless: Challenges and opportunities," *IEEE Journal on Selected Areas in Communications*, vol. 32, no. 9, pp. 1637–1652, 2014.

[11] G. Liu, F. R. Yu, H. Ji, V. C. M. Leung, and X. Li, "In-band full-duplex relaying: A survey, research issues and challenges," *IEEE Communications Surveys Tutorials*, vol. 17, no. 2, pp. 500–524, 2015.

[12] Z. Zhang, K. Long, A. V. Vasilakos, and L. Hanzo, "Full-duplex wireless communications: Challenges, solutions, and future research directions," *Proceedings of the IEEE*, vol. 104, no. 7, pp. 1369–1409, 2016.

[13] K. E. Kolodziej, B. T. Perry, and J. S. Herd, "In-band full-duplex technology: Techniques and systems survey," *IEEE Transactions on Microwave Theory and Techniques*, vol. 67, no. 7, pp. 3025–3041, 2019.

[14] I. F. Akyildiz, S. Nie, S.-C. Lin, and M. Chandrasekaran, "5G roadmap: 10 key enabling technologies," *Computer Networks*, vol. 106, pp. 17–48, 2016.

[15] M. Amjad, F. Akhtar, M. H. Rehmani, M. Reisslein, and T. Umer, "Full-duplex communication in cognitive radio networks: A survey," *IEEE Communications Surveys Tutorials*, vol. 19, no. 4, pp. 2158–2191, 2017.

[16] E. Aryafar, M. A. Khojastepour, K. Sundaresan, S. Rangarajan, and M. Chiang, "MIDU: Enabling MIMO full duplex," in *Proc. ACM MobiCom 2012*, p. 257–268, 2012.

[17] T. Riihonen, S. Werner, and R. Wichman, "Mitigation of loopback self-interference in full-duplex MIMO relays," *IEEE Transactions on Signal Processing*, vol. 59, no. 12, pp. 5983–5993, 2011.

[18] D. Bharadia, E. McMilin, and S. Katti, "Full duplex radios," in *Proceedings of the ACM SIGCOMM 2013 Conference on SIGCOMM*, SIGCOMM '13, (New York, NY, USA), p. 375–386, 2013.

[19] M. Duarte, C. Dick, and A. Sabharwal, "Experiment-driven characterization of full-duplex wireless systems," *IEEE Transactions on Wireless Communications*, vol. 11, no. 12, pp. 4296–4307, 2012.

[20] M. Jain, J. I. Choi, T. Kim, D. Bharadia, S. Seth, K. Srinivasan, P. Levis, S. Katti, and P. Sinha, "Practical, real-time, full duplex wireless," in *Proc. ACM MobiCom 2011*, p. 301–312, 2011.

[21] Y. Zeng, Y.-C. Liang, A. T. Hoang, and R. Zhang, "A review on spectrum sensing for cognitive radio: Challenges and solutions," *EURASIP Journal on Advances in Signal Processing*, no. 1, pp. 1–15, 2010.

[22] T. Yucek and H. Arslan, "A survey of spectrum sensing algorithms for cognitive radio applications," *IEEE Communications Surveys Tutorials*, vol. 11, no. 1, pp. 116–130, 2009.

[23] N. Han, S. Shon, J. H. Chung, and J. M. Kim, "Spectral correlation based signal detection method for spectrum sensing in IEEE 802.22 WRAN systems," in *2006 8th international conference advanced communication technology*, vol. 3, pp. 6–pp, IEEE, 2006.

[24] H. Tang, "Some physical layer issues of wide-band cognitive radio," *IEEE International Symposium on New Frontiers in Dynamic Spectrum Access Networks 2005*, pp. 151–159, 2005.

[25] D. Cabric, A. Tkachenko, and R. W. Brodersen, "Spectrum sensing measurements of pilot, energy, and collaborative detection," in *2006 IEEE Military Communications Conference*, pp. 1–7, 2006.

[26] E. Axell, G. Leus, E. G. Larsson, and H. V. Poor, "Spectrum sensing for cognitive radio : State-of-the-art and recent advances," *IEEE Signal Processing Magazine*, vol. 29, no. 3, pp. 101–116, 2012.

[27] S. Atapattu, C. Tellambura, and H. Jiang, "Energy detection based cooperative spectrum sensing in cognitive radio networks," *IEEE Transactions on Wireless Communications*, vol. 10, no. 4, pp. 1232–1241, 2011.

[28] F. Awin, E. Abdel-Raheem, and K. Tepe, "Blind spectrum sensing approaches for interweaved cognitive radio system: A tutorial and short course," *IEEE Communications Surveys Tutorials*, vol. 21, no. 1, pp. 238–259, 2019.

[29] A. Ghasemi and E. S. Sousa, "Spectrum sensing in cognitive radio networks: requirements, challenges and design trade-offs," *IEEE Communications Magazine*, vol. 46, no. 4, pp. 32–39, 2008.

[30] I. F. Akyildiz, B. F. Lo, and R. Balakrishnan, "Cooperative spectrum sensing in cognitive radio networks: A survey," *Physical Communication*, vol. 4, no. 1, pp. 40 – 62, 2011.

[31] B. C. Terry, A. Orange, N. Patwari, S. Kasera, and J. Van Der Merwe, "Spectrum monitoring and source separation in powder," in *Proceedings of the 14th International Workshop on Wireless Network Testbeds, Experimental Evaluation & Characterization*, p. 25–32, 2020.

[32] S. Choi, A. Cichocki, H.-M. Park, and S.-Y. Lee, "Blind source separation and independent component analysis: A review," *Neural Information Processing-Letters and Reviews*, vol. 6, no. 1, pp. 1–57, 2005.

[33] M. S. Pedersen, J. Larsen, U. Kjems, and L. C. Parra, "Convolutive blind source separation methods," in *Springer Handbook of Speech Processing*, pp. 1065–1094, Springer, 2008.

[34] G. R. Naik and D. K. Kumar, "An overview of independent component analysis and its applications," *Informatica*, vol. 35, no. 1, 2011.

[35] S. M. Kay, *Fundamentals of statistical signal processing: estimation theory*. Prentice-Hall, Inc., 1993.

[36] J. F. Cardoso and A. Souloumiac, "Blind beamforming for non-Gaussian signals," *IEEE Proceedings F - Radar and Signal Processing*, vol. 140, no. 6, pp. 362–370, 1993.

[37] E. Bingham and A. Hyvärinen, "A fast fixed-point algorithm for independent component analysis of complex valued signals," *International Journal of Neural Systems*, vol. 10, pp. 1–8, 03 2000.

[38] M. Novey and T. Adali, "Adaptable nonlinearity for complex maximization of nongaussianity and a fixed-point algorithm," in *2006 16th IEEE Signal Processing Society Workshop on Machine Learning for Signal Processing*, pp. 79–84, 2006.

[39] H. Akoglu, "User's guide to correlation coefficients," *Turkish Journal of Emergency Medicine*, vol. 18, no. 3, pp. 91–93, 2018.

[40] M. Ettus and M. Braun, "The universal software radio peripheral (USRP) family of low-cost SDRs," in *Opportunistic Spectrum Sharing and White Space Access*, pp. 3–23, 2015.

[41] TAOGLAS, "Specification of the wideband 4G LTE I-Bar antenna," 2017.

[42] P. Hillyard, A. Luong, and N. Patwari, "Highly reliable signal strength-based boundary crossing localization in outdoor time-varying environments," in *2016 15th ACM/IEEE International Conference on Information Processing in Sensor Networks (IPSN)*, pp. 1–12, 2016.